Journal of Electroanalytical Chemistry 661 (2011) 1–7

Contents lists available at ScienceDirect

Journal of Electroanalytical Chemistry

journal homepage: www.elsevier.com/locate/jelechem

Comparative behavior of conjugates of tantalum phthalocyanines with gold nanoparticles or single walled carbon nanotubes towards bisphenol A electrocatalysis

Vongani P. Chauke, Edith Antunes, Tebello Nyokong *

Department of Chemistry, Rhodes University, Grahamstown 6140, South Africa

ARTICLE INFO

Article history:
Received 15 April 2011
Received in revised form 3 June 2011
Accepted 14 June 2011
Available online 6 July 2011

Keywords:
Gold nanoparticles
Tantalum phthalocyanine
Bisphenol A
Single walled carbon nanotubes

ABSTRACT

The characterization of tantalum phthalocyanine conjugates with gold nanoparticles and single wall carbon nanotubes as well as their electrocatalytic oxidation of bisphenol A is hereby presented. The formation of the conjugates was confirmed by X-ray diffraction and transmission electron microscope techniques. Single walled carbon nanotube conjugates of TaPc complexes showed the best catalysis as well as less passivation for bisphenol A detection and significant recovery of ~98% compared to gold nanoparticle conjugates.

1. Introduction

Metallophthalocyanines (MPc) are known to act as good electrocatalysts for many analytes when employed to modify electrode surfaces [1–4]. Similarly, gold nanoparticles (AuNPs) have found applications in electrochemical sensing [5,6] due to their high surface-to-volume ratio, which gives them high sensitivity over their bulk gold counterparts [5–8]. Thus the combination of MPcs and AuNPs may enhance the catalytic activity compared to when these extraordinary catalysts are used separately. To illustrate this, conjugates of AuNPs with MPcs will be employed for the electrocatalytic oxidation of bisphenol A (BPA) in this work. Alkylthio TaPc conjugates with AuNPs have been characterized [9]. In this work, tantalum phthalocyanine complex (**3**) substituted at the peripheral positions with an aryl substituent (2-mercaptopyridine, Scheme 1) will be conjugated to AuNPs, and its behavior compared with that of complex **4** substituted with alkyl substituents. The two TaPc derivatives (**3** and **4**) will also be adsorbed onto single walled carbon nanotubes (SWCNTs). The aim is to compare AuNPs and SWCNTs towards reducing electrode passivation during the detection of BPA. The central metal Ta was chosen because of the possibility of multiple oxidation states, and the fact that electrocatalytic behavior of TaPc has been relatively unexplored [9]. This is due to the difficulty in the synthesis of these complexes. The mercaptopyridine group was chosen since it is a bulky group which may prevent aggregation of TaPc derivative. The presence of the electron donating thio group will make oxidation easier, hence improve electrocatalysis. The conjugates (TaPc-AuNPs or TaPc-SWCNT) are characterized by transmission electron microscopy (TEM), X-ray diffraction (XRD) and cyclic voltammetry and employed for BPA detection.

Single walled carbon nanotubes (SWCNT) are one dimensionless nanowires that are either metallic or semi conducting and they readily accept charges which they transport along their tubular axis [10–12]. Their remarkable properties have encouraged their use in electrochemical devices for electron-transfer processes [13–15]. Carbon nanotubes have been non-covalently functionalised using porphyrins [16] and metallophthalocyanines [17,18] through π-π interactions. In this work, TaPc complexes (**3** and **4**) were non-covalently bonded to carbon nanotubes to form **3**-SWCNT and **4**-SWCNT conjugates and these were employed for the electrooxidation of BPA.

Biphenol A, is a type of estrogen present in the environment, and it can have harmful effects on the endocrine systems of humans and wild animals [19–21]. Electrochemical methods have been explored for the detection of BPA [22–24]. However, the major drawback with the oxidation of phenolic type compounds on bare electrodes is the inevitable formation of dimers which passivate the electrode surface resulting in low oxidation currents [1]. We have recently reported [9] that TaPc derivatives and their conjugates with AuNPs showed catalytic activity towards BPA. We also

* Corresponding author. Fax: +27 46 622 5109.
E-mail address: T.nyokong@ru.ac.za (T. Nyokong).

1572-6657/$ - see front matter © 2011 Elsevier B.V. All rights reserved.
doi:10.1016/j.jelechem.2011.06.019

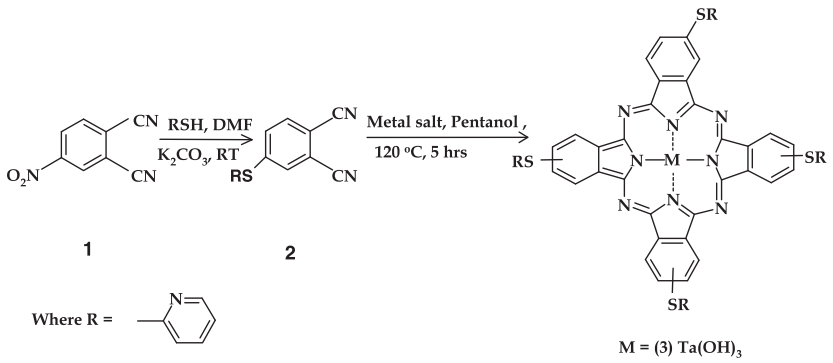

Scheme 1. Synthetic route for the tantalum phthalocyanine complex (**3**).

reported on the use of nickel tetraamino phthalocyanine [Ni(II)-TAPc] for BPA detection, which showed extensive passivation of the electrode [22]. Yin et al. [23,24] reported on the use of cobalt phthalocyanine carbon paste electrode (CPE) and multiwalled carbon nanotubes (MWCNT) – cobalt phthalocyanines – silk fibroin films for BPA detection, with improved stability. The current work is aimed at using a Au electrode modified with conjugates of TaPc with SWCNT or AuNPs. The electrode is modified by a simple adsorption method. The aim is to minimize passivation, hence improve electrode re-usability. The effects of AuNPs or SWCNT on the electrocatalytic behavior of TaPc derivatives are compared.

2. Experimental

2.1. Materials

Toluene and acetonitrile were purchased from Saarchem. Bisphenol A (BPA) was purchased from Sigma Aldrich. Ultra pure water of 18.2 MΩ cm resistivity {and total organic content (TOC) of 4 ppb} was from a Milli-Q Water system. pH 12 phosphate buffer solutions were prepared from KH_2PO_4 and Na_2HPO_4, and NaOH was used to adjust the pH. Gold nanoparticles (and AuNP-MPc conjugates) were synthesised as described recently [9]. The synthesis of **4** (Fig. 1) was reported in Ref. [25].

2.2. Equipment

Transmission electron microscope (TEM) images were obtained using a JEOL JEM 1210 transmission electron microscope at 100 kV accelerating voltage. A few drops of the solutions of the samples were placed on carbon coated 300 mesh grids and were left to dry for about 30 s. X-ray powder diffraction (XRD) patterns were recorded on a Bruker D8, Discover equipped with a proportional Lynx Eye Detector using Cu Kα radiation (λ = 1.5405 Å, nickel filter). Data were collected in the range from $2\theta = 5°$ to 60°, scanning at 1° min^{-1} with a filter time-constant of 2.5 s per step and a slit width of 6.0 mm. Samples were placed on a silicon wafer slide. The X-ray diffraction data were treated using Eva (evaluation curve fitting) software. Baseline correction was performed on each diffraction.

Cyclic voltammetry (CV) experiments were performed using Autolab Potentiostat/Galvanostat model 263A (Princeton Applied research) driven by the Electrochemistry Powersuit software, using a conventional three-electrode system. Spectroelectrochemical data was recorded using an optically transparent thin-layer electrochemical (OTTLE) cell which was connected to a Bioanalytical System (BAS) CV 27 voltammograph. The electrodes for spectroelectrochemical studies are Pt mesh working and counter electrodes, and a Ag|AgCl pseudo reference electrode.

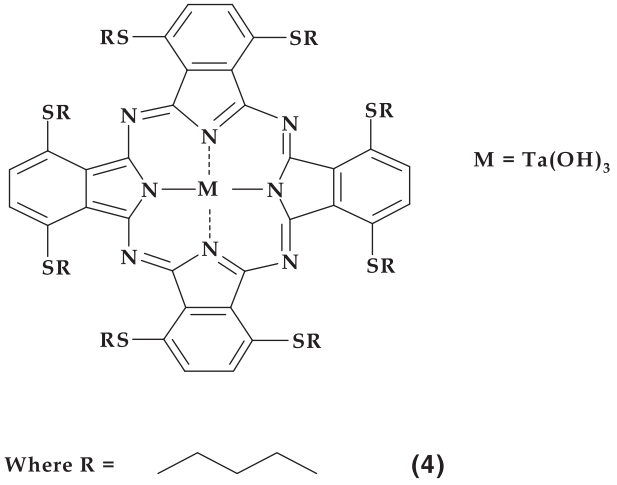

Fig. 1. Molecular structures of complex 4.

2.3. Electrochemical methods

The gold disk electrode surface was polished in aqueous slurry of alumina on sic-emery paper and subjected to ultrasonic vibration in absolute ethanol to remove residual alumina. The electrode was then etched in hot 'piranha' solution (1:3 v/v 30% H_2O_2 and concentrated H_2SO_4) for 2 min and rinsed with excess Millipore water. The electrode was then scanned in 0.5 M H_2SO_4 between −0.5 and 1.5 V vs Ag|AgCl to obtain a reproducible scan.

The working electrodes were either bare or Au disk (1.6 mm diameter) modified with the following complexes: AuNPs, **3**, **3**-AuNPs, **4**-AuNPs, SWCNT, **3**-SWCNT or **4**-SWCNT. Respectively, silver–silver chloride (Ag|AgCl) and platinum wire were used as pseudo-reference and counter electrodes. The potential of the pseudo reference electrode was less than that of Ag|AgCl (3 M KCl) by 0.015 ± 0.003 V. The modification of the working Au electrode was achieved using the drop – dry method, where a drop of the complex of interest (AuNPc or TaPc-AuNPs conjugates dissolved in toluene; or SWCNT or TaPc-SWCNT suspended in $CHCl_3$ following sonication) was placed on the electrode surface and left to dry for ∼10 min in the oven. This allowed for adsorption of the complexes onto the electrode surface. The removal of the excess catalyst was accomplished by rinsing the electrode in toluene (for AuNPs and their conjugates) or $CHCl_3$ (for SWCNT or their conjugates) followed by acetone before use.

All solutions were de-aerated by bubbling argon preceding the experiments and the argon atmosphere was maintained throughout the experiments. A stock solution of 1×10^{-3} mol L^{-1} bisphenol A was prepared in a mixture of deionised water/acetonitrile (60:30 v/v). This solvent mixture was employed due to the lack

of solubility of BPA in water alone. For practical BPA applications, samples were obtained from a local food market in Grahamstown. Two types of plastic products were used; microwave plastic from meat package and a baby feeding bottle. Both plastic products were washed thoroughly with water and soap to remove blood stains, animal fat and other impurities. The plastic products were then placed in a big bowl, separately, and exposed to high microwave power for 10 min [24]. This was repeated three times on different days. The BPA concentrations were determined using the standard addition method.

2.4. Synthesis of (2-mercaptopyridine)pthalocyaninato tantalum (IV) butoxide (**3**), Scheme 1

Under a stream of nitrogen, a mixture of tantalum (V) butoxide (0.66 g, 1.21 mmol), 3-(2-mercaptopyridine)phthalonitrile (**2**, 0.25 g, 1.05 mmol), DBU (1.66 mL, 12 mmol) and 1-pentanol (10 mL) was stirred at 160 °C for 5 h. After cooling, methanol was added to the solution. The resulting precipitate was filtered and washed twice with methanol. Column chromatography over silica was done using $CHCl_3$ as eluent.

Yield: 0.25 g (42%). UV/Vis (Toluene): λ_{max} (nm) (log ε) 335 (4.59) 620(4.15) 688(5.74), 710 (5.79). IR (KBr): ν_{max}/cm^{-1}; 3063 (Ar-H), 1560 (C=C), 1523, 1452, 1345, 1201, 1307, 1285, 1201, 1109, 1095 (C—S—C), 910, (Ta-O). ^{1}H NMR ($CDCl_3$): δ, ppm: 8.32–9.33 (m, 8H, Pc-H), 7.71–8.50 (m, 4H, Pc-H), 6.70–7.30 (m, 16H, Pyridyl-H), Calc. for $C_{52}H_{31}N_{12}S_4O_4Ta$: C 52.16; H 2.61; N 14.04; S 10.71; Found: C 52.09, H 3.04, N 14.14, S 10.45. MALDI-TOF MS *m/z*: Calcd: 1197 amu. Found: [M-Ta] 965 amu.

2.5. Synthesis of TaPc-SWCNT conjugates

The SWCNT were purified by following methods described previously in literature [26] with modification as follows: SWCNT (150 mg) were suspended in a mixture of concentrated HNO_3: H_2SO_4 (1:3) and stirred at 70 °C for 2 h. The SWCNTs were subsequently washed with water and dried in the oven overnight at 70 °C. The **3**-SWCNT and **4**-SWCNT conjugates were formed by mixing complexes **3** or **4** (3.5 mg) and SWCNT (1.0 mg) in $CHCl_3$ (1.5 mL) and stirred for ~12 h. Adsorption of TaPc derivatives onto SWCNT is expected due to π–π interactions between the two.

2.6. Synthesis of AuNPs and TaPc-AuNP conjugates

The synthesis of gold nanoparticles (using phase transfer agent TOABr as a protecting ligand) was achieved following the method described by Brust et al. [27] and as reported before [28]. Briefly gold (III) chloride trihydrate solution (25 mmol L^{-1}, 4 mL) was vigorously stirred with a solution of TOABr (85 mmol L^{-1}, 6 mL) in toluene until all the gold chloride was transferred to the organic phase, as judged by the change of color from orange to red [27,28]. An aqueous solution of a reducing agent $NaBH_4$ (3.6×10^{-2} mol L^{-1}) was then added drop-wise over a period of 10 min. The mixture was then stirred vigorously for 30 min. The organic phase was separated and washed with water. Solid complexes of conjugates of **3** and **4** with AuNPs were synthesized by mixing the two, allowing time (~28–30 h) for the MPcs to react with the gold nanoparticles. The solvent (toluene) was then evaporated. The uncoordinated TaPc derivatives were removed in a size-exclusion column (bio-beads).

3. Results and discussion

3.1. Characterization of complex **3**

Scheme 1 gives the synthetic pathways for **3**. Column and preparative thin layer chromatography with silica gel were employed to obtain the pure product from the reaction mixtures. The synthesised complex (**3**) is soluble in organic solvents such as dichloromethane, chloroform, chloronaphthalene, dimethylformamide (DMF) and dimethylsulfoxide (DMSO).

The new complex was found to be pure by ^{1}H NMR with all the substituents and ring protons observed in their respective regions. The metal salt employed for synthesis of complex **3** was tantalum butoxide, however the axial ligand obtained is hydroxide as a result of the purification process. Elemental analyses and mass spectral data were consistent with the structure of the complex.

The loss of symmetry is observed for complex **3** as judged by the split Q band, Fig. 1 (Supporting material), even though this complex is substituted at peripheral positions. This is due to the large size of the Ta central metal which lies more out of the plane of the ring when compared to the other central metals.

The cyclic voltammogram (CV) of TaPc complex (**3**) is shown in Fig. 2 in DMF containing 0.1 M $TBABF_4$. Reduction processes labelled **II** and **III** at half-wave ($E_{1/2}$) potentials of −0.57 and −0.99 V vs Ag|AgCl, respectively were observed. The ΔE values of 84 and 90 mV for couples **II** and **III** suggests reversibility (ΔE for ferrocene standard was 80 mV). Process **I** is irreversible and is observed at 0.86 V. Compared to octa pentathio alpha substituted TaPc complex (**4**) and unsubstituted TaPc in Table 1, [25,29] complex **3** is easier to reduce that the former but more difficult to reduce than the latter. The ease of reduction of **3** compared to unsubstituted TaPc is due to the thio substituents which are electron donating hence making reduction more difficult. The assignments of the redox processes for **3** are based on spectroelectrochemistry.

Fig. 2 (Supporting material) shows the absorption spectral changes observed on applying potentials more negative than potentials of couple **II** (−0.57 V vs Ag|AgCl), a shift of the split Q

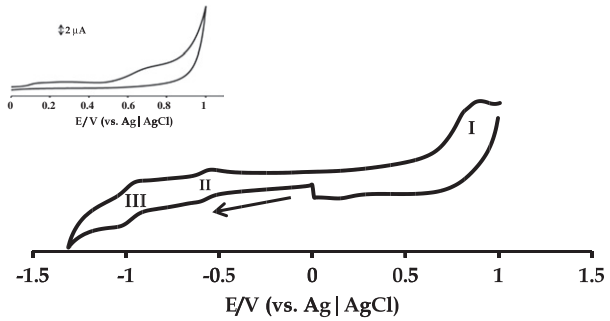

Fig. 2. Cyclic voltammogram of complex **3** in DMF containing 0.1 M $TBABF_4$. Scan rate = 100 mV/s. Inset: Complex **3** adsorbed onto Au electrode.

Table 1
Electrochemical data (half-wave potential, $E_{½}$, unless otherwise stated) for TaPc derivatives in DMF containing 0.1 M $TBABF_4$. (Potentials vs Ag|AgCl.

Complex	$Ta^{V}Pc^{-2}$/ $Ta^{IV}Pc^{-2}$	$Ta^{IV}Pc^{-2}$/ $Ta^{IV}Pc^{-3}$	$Ta^{IV}Pc^{-3}$/ $Ta^{IV}Pc^{-4}$	Oxidation processes	Refs.
3	−0.57	−0.99		0.86	TW
4	−0.74	−1.13		0.37, 0.57	[25]
TaPc	−0.31	−0.48	−0.94	075	[29]

[a]TW = This work.

band from 667 to 701 nm to 601 and 664 nm was observed. The combination of aggregation and loss of symmetry may have resulted in broadening of the spectra in Fig. 2a (Supporting material). Isosbestic points were diffuse, possibly to due axial ligand exchange and aggregation. Typically, the changes in Fig. 2a (Supporting material) are due to redox processes occurring at the central metal [30], since there is no drastic decrease in intensity of the Q band. Therefore, process **II** is attributed to the reduction $Ta^{V}Pc^{-2}$ to $Ta^{IV}Pc^{-2}$. Further reduction at potentials of process **III** (−0.99 V vs Ag|AgCl), Fig. 2b (Supporting material), resulted in a decrease in the intensity of the Q band and the appearance of new peaks at ~560 nm. The appearance of new bands between 500 and 600 nm is typical of ring reduction processes [31], i.e. $Ta^{IV}Pc^{-2}$ is reduced to $Ta^{IV}Pc^{-3}$. Oxidation is expected only on the ring for $Ta^{IV}Pc$ complexes, hence process **I** is assigned to the formation of $Ta^{IV}Pc^{-1}$.

3.2. Characterization of MPc-AuNPs and MPc-SWCNT

Fig. 3 shows the TEM images of AuNPs (Fig. 3a) and **3**-AuNPs (Fig. 3b). Fig. 3a illustrates the spherical nature of the AuNPs and in Fig. 3b, the TaPc appears to be around the gold nanoparticles, as evidenced by the dark areas on the AuNP. It is possible that the MPc complexes are simply adsorbed onto the AuNPs.

Similarly, the SWCNT were characterized and visualized using TEM. Fig 4a shows the SWCNT alone with rod-like shapes and closely packed together. Fig. 4b shows that on interaction of SWCNT with complex **4**, the spaces between rod-like SWCNTs seem to be decreased due to the presence of complex **4** on the SWCNTs.

To determine the size of the gold nanoparticles, X-ray diffraction (XRD) technique was employed. Debye–Scherrer [32] (Eq. (1)) was used to calculate the size of the gold nanoparticles and MPc conjugates.

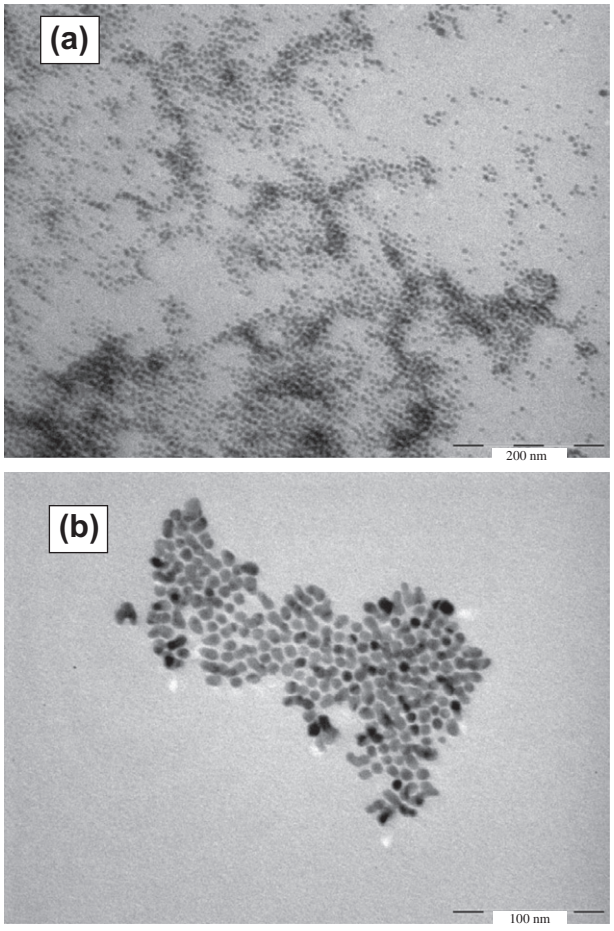

Fig. 3. TEM images of (a) AuNps in toluene (b) AuNPs modified with complex **3.**

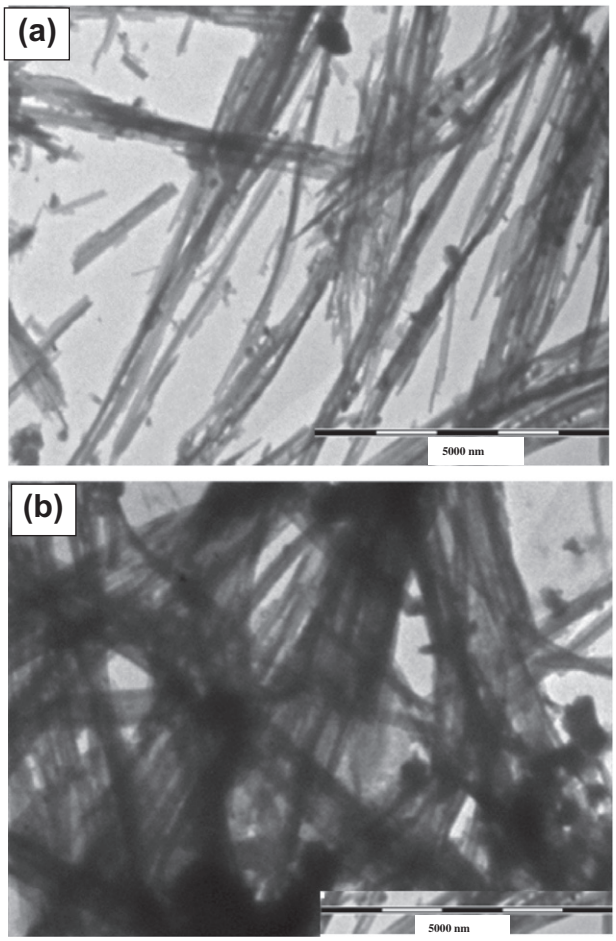

Fig. 4. TEM images of (a) SWCNT in toluene (b) SWCNT modified with complex **4.**

$$d\text{Å} = \frac{k\lambda}{\beta Cos\theta} \quad (1)$$

where k is an empirical constant equal to 0.9, γ is the wavelength of the X-ray source, (1.5405 Å), β is the full width at half maximum of the diffraction peak, and θ is the angular position of the peak. Fig. 3 (Supporting material) shows the XRD pattern for the AuNPs employed in this work. The average size for the AuNPs was then worked out to be 10.1 nm, using the peak that fits the structure database reflection for gold.

3.3. Electrode modification using MPcs and their conjugates with AuNPs or SWCNT

The cyclic voltammograms of all the complexes (adsorbed on Au electrode) used in this work were obtained in pH 12 phosphate buffer. The bare or modified electrodes were scanned between −1.2 V and 1.0 V vs Ag|AgCl. Gracia et al. [33] have reported the use of adsorbed AuNPs onto Au disk electrode where they observed no gold oxidation for AuNPs below 0.6 V on indium tin oxide (ITO) coated glass. Similarly, AuNPs do not show any gold oxidation on Au disk electrodes [9,34,35] below 0.6 V. The oxidation peak of AuNPs has been reported at 1.28 V (vs saturated calomel electrode) and the reduction peak at 0.81 V [33]. We reported the AuNP oxidation at 0.99 V in pH 7.4 buffer and the subsequent reduction at 0.36 V vs Ag|AgCl [9]. Fig. 2 (inset) shows cyclic voltammogram

of adsorbed complex **3** on Au disk. The AuNP oxidation occurs at potentials more positive than those in Fig. 2 (inset), and has been left out, hence the subsequent reduction will not be observed. The broad oxidation process is observed between 0.6 and 0.8 V in Fig. 2 (inset) and is attributed to ring oxidation process in comparison with solution voltammograms (Fig. 2). Only ring based oxidations are expected in TaPc complexes. The peak for TaPc derivatives for complex **4** was observed at 0.5 V, in the presence of AuNPs and SWCNTs the TaPc oxidation peaks are observed at lower potentials 0.3–0.4 V.

The surface coverages were calculated for the adsorbed complexes by first determining the effective area of the Au electrode using the $[Fe(CN)_6]^{3-/4-}$ redox system and applying the Randles–Sevcik (Eq. (2)) for a reversible process [36]:

$$I_{pa} = (2.69 \times 10^5) n^{3/2} D^{1/2} v^{1/2} A C_o \quad (2)$$

where D and C_o are the diffusion coefficient and bulk concentration of the redox probe (1 mM $K_3[Fe(CN)_6]$), respectively. n = 1 is the number of electrons transferred, v is the scan rate and A is the effective surface area. From the D value for $K_3[Fe(CN)_6]$ = 7.6×10^{-6} cm^2 s^{-1} [37], the surface roughness of the electrode was found to be 1.36 (ratio of I_{pa} experimental/I_{pa} theoretical) corresponding to a real electrode area of 0.0274 cm^2 (roughness factor × theoretical surface area = 0.0201 cm^2).

The surface coverages (Γ) of modified electrodes were estimated by integrating the charge under the MPc (Fig. 2 insert as an example) using the following equation [36].

$$\Gamma = \frac{Q}{nFA} \quad (3)$$

where Q (C) is the charge under the metal oxidation peak, n (=1) is the number of electrons, A is the effective area of the electrode (calculated from Eq. (2)) and F is Faraday's constant (95,485 C mol^{-1}).

The determined surface coverages of the AuNPs, **3**, **4**, **3**-AuNP and **4**-AuNP electrodes ranged from 1.54×10^{-10} to 5.25×10^{-10} mol cm^{-2}, Table 2. Surface coverages were was calculated for SWCNT, **3**-SWCNT and **4**-SWCNT using the method described above and were found to be 1.88×10^{-10}, 3.39×10^{-10} and 2.55×10^{-10}, respectively, Table 2. The values for TaPc-AuNP or TaPc-SWCNT represent an increase compared to AuNP or SWCNT alone. Also larger surface coverages are obtained for TaPc-AuNP compared to TaPc-SWCNT. The expected monolayer coverage value for phthalocyanines lying flat on the electrode is 1×10^{-10} mol cm^{-2} [38]. This suggests multilayer coverage for the TaPc complexes alone.

3.4. Electrocatalysis of bisphenol A using TaPc derivatives in conjugation with AuNPs or SWCNT

Fig. 5 shows the CVs for the electrocatalytic oxidation of BPA in pH 12 phosphate buffer using TaPc derivatives and their conjugates with AuNPs. The AuNPs oxide formation and its stripping

Table 2
Cyclic voltammetry parameters for surface coverage and BPA detection.

Electrode modifier	Surface coverage Γ, mol cm^{-2} (MPc)	Ep (V) vs Ag|AgCl (BPA oxidation)	Current (Amps)
AuNPs	2.87×10^{-10}	0.45	3.24×10^{-6}
SWCNT	1.88×10^{-10}	0.20	5.25×10^{-6}
3	1.54×10^{-10}	0.22	2.03×10^{-6}
3-AuNPs	5.25×10^{-10}	0.38	4.20×10^{-6}
3-SWCNT	3.39×10^{-10}	0.16	5.12×10^{-6}
4	1.98×10^{-10}	0.19	3.24×10^{-6}
4-AuNP	4.51×10^{-10}	0.41	5.98×10^{-6}
4-SWCNT	2.55×10^{-10}	0.19	3.26×10^{-5}

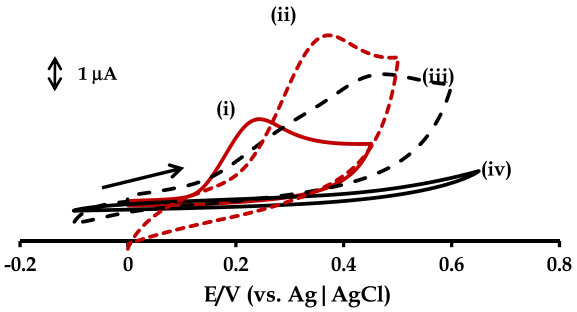

Fig. 5. Cyclic voltammograms recorded in 7×10^{-3} mol L^{-1} BPA in pH 12 phosphate buffer: (a) (i) **3**, (ii) **3**-AuNPs, (iii) AuNPs, (iv) bare gold electrode.

are not expected at the potential range shown in Fig. 5, as explained above, thus all the peaks are due to BPA oxidation. The bare electrode, Fig. 5iv, showed no detection of BPA. Catalytic behavior is characterized by an increase in currents and improvement in the potential (to be precise, shift to less positive values during oxidation). The TaPc complexes used in this work and their conjugates with AuNPs are able to catalyse the oxidation of BPA since peaks are observed with potentials ranging between 0.19 and 0.41 V, Table 2 for **3** or **4** and their conjugates with AuNPs, were obtained. AuNPs in the absence of TaPc derivatives were less efficient for BPA oxidation as judged by more positive potential, Table 2, Fig. 5iii. A shift of potential to more positive values for BPA oxidation was observed on **3**-AuNPs or **4**-AuNPs compared to corresponding TaPcs alone, but with increase in current for the former, Table 2. The increase in current for **3**- or **4**-AuNPs is attributed to higher surface coverage compared to corresponding TaPcs alone. The BPA detection potentials in this work were lower when compared to the reported NiTAPc containing 'O—Ni—O' bridges [22], CoPc-CPE [23] and MWNTs-CoPc [24], where there BPA oxidation potentials were 0.45 V, 0.41 V and 0.58, respectively. It is also interesting to note that 'bulk' Au electrode was not sensitive towards the oxidation of BPA; however Au in its nanosized form could catalyse the oxidation of BPA. This therefore confirms that indeed AuNPs have extraordinary catalytic properties.

Fig. 6 shows the comparative cyclic voltammetric responses of **4**-SWCNT (i), **3**-SWCNT and SWCNT (iii) towards the oxidation of BPA. The oxidation potential for the three complexes were more or less the same although the oxidation potential by **3**-SWCNT was slightly less at 0.16 V, Table 2, compared to SWCNT or **4**-SWCNT. **4**-SWCNT showed larger currents for BPA detection when compared to the rest of the electrodes in Table 2. It was interesting

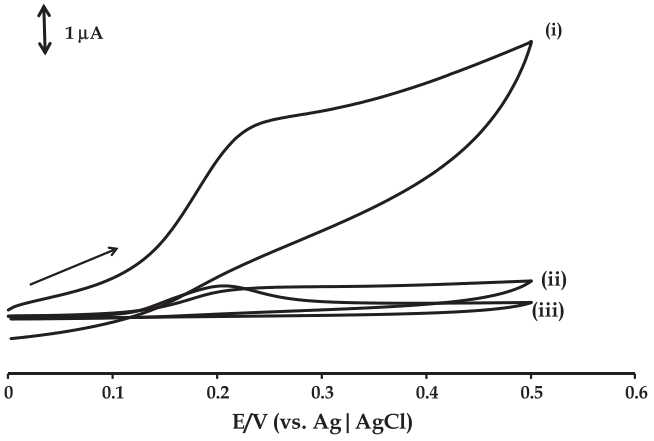

Fig. 6. Cyclic voltammograms recorded in 7×10^{-3} mol L^{-1} BPA in pH 12 phosphate buffer: (i) **4**-SWCNT, (ii) **3**-SWCNT and (iii) SWCNT.

$Ta^{V}Pc^{2-}$	→	$[Ta^{V}Pc^{1-}]^{+} + e^{-}$	Step 1
$[Ta^{V}Pc^{1-}]^{+} + R\text{-}O^{-}$	→	$R\text{-}O^{\bullet} + Ta^{V}Pc^{2-}$	Step 2
$R\text{-}O^{\bullet} + R\text{-}O^{\bullet}$	→	dimers	Step 3

Scheme 2. Proposed reaction mechanism for the electrooxidation of BPA, where R (in steps 1 and 3) represents the rest of the BPA molecule.

Table 3
Selectivity and limits of detection for the detection of BPA on TaPc complexes.

Electrode modifier	Sensitivity ($\mu A\ mmol^{-1}\ L^{1}\ cm^{-2}$)	LOD ($mol\ L^{-1}$)	Refs.
3	3.21×10^{-5}	1.02×10^{-10}	This work
3-AuNP	3.30×10^{-5}	1.87×10^{-10}	This work
3-SWCNT	3.47×10^{-4}	1.90×10^{-10}	This work
4	4.20×10^{-5}	4.78×10^{-10}	[9]
4-AuNP	4.29×10^{-5}	2.03×10^{-10}	This work
4-SWCNT	2.12×10^{-4}	1.16×10^{-10}	This work

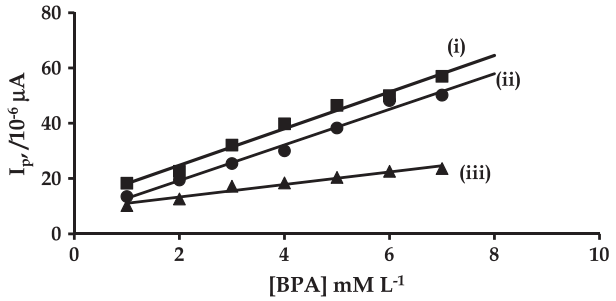

Fig. 7. Calibration curves for BPA detection (i) **4**-SWCNT, (ii) **3**-AuNPs and (iii) **3** in pH 12 phospahte buffer.

to note that the SWCNT alone showed BPA oxidation, Fig. 6, Table 2.

The mechanism (in basic media) for the oxidation of BPA is expected to be similar to that proposed for its oxidation on CoPc-CPE [23] but catalyzed by ring based oxidation processes since metal oxidations do not occur in all the complexes, Scheme 2:

Catalysis was carried out in basic media where BPA deprotonates, hence the presence of BPA anion in step 2. The catalytic oxidations occur at potentials where ring based processes occur. The oxidation of BPA forms radicals (step 2) which subsequently dimerize to form polymers as indicated in step 3.

The analysis data (sensitivity and limits of detection, Table 3) were carried out for complexes **3** and **4**, and compared to their AuNP and SWCNT conjugates (**3**-AuNPs, **3**-SWCNT, **4**-AuNPs and **4**-SWCNT). Shown in Fig. 7 are the linear plots of current vs BPA concentrations in the range of 1–8 mM for, **3**, **3**-AuNPs and **4**-SWCNT. The calculated sensitivity values were obtained from the slope of the linear plot and ranged from 3.21×10^{-5} to $2.12 \times 10^{-4}\ \mu A\ mmol^{-1}\ L^{1}\ cm^{-2}$, Table 3. The limits of detection (LoD) were determined according to literature [39], by recording the chronoamperometry (at 0.22, 0.19, 0.38, 0.16, 0.41 and 0.19 V potentials for complexes, **3, 4, 3**-AuNP, **3**-SWCNT, **4-A**uNP and **4**-SWCNT, respectively) of the modified electrode in pH 12 buffer. The LoD was then calculated by multiplying the standard deviation of the chronoamperometry current by three and then dividing the result by the gradient of the calibration curve in Fig. 7. The LoD ranged from 1.02×10^{-10} to $4.78 \times 10^{-10}\ mol\ L^{-1}$, respectively. The chronoamperometric response due to the buffer alone constitutes the background current. On adding $\sim 10^{-10}\ mol\ L^{-1}$ BPA to the buffer, the current responses were above that of the background for **4**-SWCNT. This would imply that the operational limit of detection could be very similar to the theoretical LOD obtained through the 3δ criterion. These LOD values, Table 3, are an improvement over the values reported [22] for 'O—Ni—O' oxo bridges (for *poly*-70-Ni(OH)NiTAPc, $3.68 \times 10^{-9}\ mol\ L^{-1}$), the CoPc-CPE (LoD = $1.0 \times 10^{-8}\ mol\ L^{-1}$) [23] and carbon electrode which had been modified with a multi-walled carbon nanotube-gold nanoparticle hybrid film, $3 \times 10^{-8}\ mol\ L^{-1}$ [24].

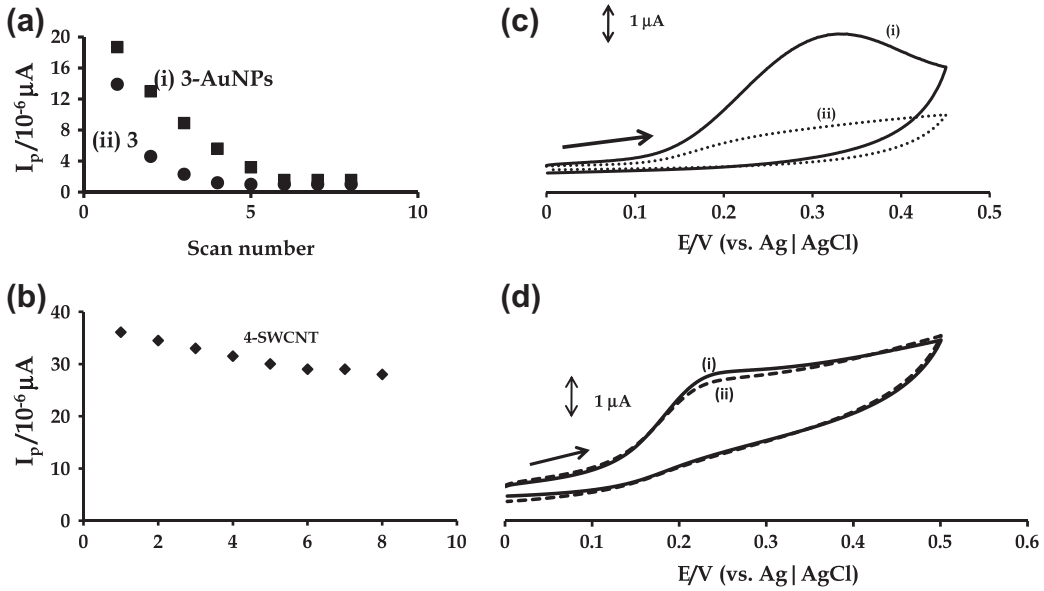

Fig. 8. Variation of peak current with scan number for the voltammetric responses in $7 \times 10^{-3}\ mol\ L^{-1}$ BPA in pH 12 phosphate buffer for (a) (i) **3**-AuNP and (ii) **3,** (b) **4**-SWCNT. (c) and (d) are the cyclic voltammograms recorded in $7 \times 10^{-3}\ mol\ L^{-1}$ BPA for the re-use of **3**-AuNPs and **4**-SWCNT, respectively. (i) and (ii) in (c) and (d) are the first scan and the scan following re-use and rinsing 0.1 M NaOH, respectively.

For real samples, the BPA concentration for the microwave plastics obtained from a local supermarket was determined using complex **3** as an example since it gave the lowest LOD for the BPA standard. A standard addition method was employed, where the BPA concentration in the plastic was found to be 1.89 μM. No BPA was detected in the feeding bottle.

3.5. Electrode stability

Phenolic type compounds are notorious for poisoning electrode surfaces. This is as a result of the formation of polymer-like structures and hydroquinones when oxidized, which subsequently block the electrode surface [1,2]. Electrode passivation is illustrated by a drastic decrease in current, shown Fig. 8a where a drop in I_p with increase in scan number is observed, indicating passivation. In the presence of AuNPs, however, the drop in current was gradual, implying that the presence of AuNPs reduces passivation. The electrodes could be partially regenerated by rinsing in 0.1 M NaOH as shown in Fig. 8c which is illustrative of weak recovery, where (i) is the first scan and (ii) is the cyclic voltammogram of BPA after rinsing in 0.1 M NaOH for complex **3**. The recovery was roughly 22%.

Less passivation was observed on **4**-SWCNT Au modified electrodes, Fig. 8b. This reiterates the fact mentioned earlier that less fouling is experienced in the presence of SWCNT. Furthermore, recovery by rinsing in concentrated NaOH solution was almost up to ~98% (Fig. 8d), again proving that SWCNT are remarkable.

4. Conclusions

The electrocatalytic oxidation of BPA was observed on electrodes modified with TaPc complexes and their AuNPs or SWCNT conjugates. The presence of AuNPs or SWCNT increases sensitivity significantly and interestingly AuNPs (and SWCNT) alone showed BPA detection which was not obtained on the bare Au electrode. Passivation was inevitable; however, in the presence of AuNPs the process of passivation was gradual. Regeneration of the electrode surface was achieved partially by rinsing in 0.1 M NaOH. **4**-SWCNT showed very high activity towards BPA analysis. Both **3**-SWCNT and **4**-SWCNT showed minimal electrode fouling, hence improved recovery.

Acknowledgements

This work was supported by the Department of Science and Technology (DST) and National Research Foundation (NRF), South Africa through DST/NRF South African Research Chairs Initiative for Professor of Medicinal Chemistry and Nanotechnology as well as Rhodes University.

Appendix A. Supplementary material

Supplementary data associated with this article can be found, in the online version, at doi:10.1016/j.jelechem.2011.06.019.

References

[1] T. Nyokong, in: J.H. Zagal, F. Bedioui, J.-P. Dodelet (Eds.), N4-Macrocyclic Metal Complexes, Springer, New York, 2006.
[2] C.A. Caro, F. Bedioui, J. Zagal, Electrochim. Acta. 47 (2002) 1489.
[3] C.A. Caro, F. Bedioui, M.A. Paez, G.I. Cárdenas-Jirón, J.H. Zagal, J. Electrochem. Soc. 151 (2004) E32.
[4] J.H. Zagal, S. Griveau, J.F. Silva, T. Nyokong, F. Bedioui, Coord. Chem. Rev. 254 (2010) 2755–2791.
[5] G. Maduraiveeran, R. Ramaraj, Electrochem. Commun. 8 (2007) 2051.
[6] J. Zhang, Y. Wang, R. Lv, L. Xu, Electrochim. Acta. 55 (2010) 4039.
[7] F. Matsumoto, K. Tokuda, T. Ohsak, Electrochem. Commun. 4 (2002) 288.
[8] C.R. Raj, K.V. Gobi, T. Ohsak, Bioelectrochem. 51 (2001) 181.
[9] V. Chauke, W. Chidawanyika, T. Nyokong, Electroanalysis 23 (2011) 487.
[10] S. Banerjee, S.S. Wong, Nano Lett. 2 (2002) 49.
[11] B. Ballesteros, S. Campidelli, G. De la Torre, C. Ehli, D.M. Guldi, M. Prato, T. Torres, Chem. Commun. (2007) 2950.
[12] M. Inagaki, K. Kaneto, T. Nishizawa, Carbon 42 (2004) 1401.
[13] P.J. Britto, K.S.V. Santhanam, P.M. Ajayan, Bioelectrochem. Bioenerg. 41 (1996) 121.
[14] A. Salimi, R. Hallaj, Talanta 66 (2005) 967.
[15] J. Kruusma, N. Mould, K. Jurkschat, A. Crossley, C.E. Banks, Electrochem. Commun. 9 (2007) 2330.
[16] R.J. Chen, Y. Zhang, D. Wang, H. Dai, J. Am. Chem. Soc. 123 (2001) 3838.
[17] J.F. Silva, S. Griveau, C. Richard, J.H. Zagal, F. Bedioui, Electrochem. Commun. 9 (2007) 1629.
[18] H. Murakami, G. Nakamuri, T. Nomura, T. Miyamoto, N. Nakashima, J. Porphyrins Phthalocyanines 11 (2007) 418.
[19] H. Sanbe, J. Haginaka, J. Pharm. Biomed. Anal. 30 (2002) 1835.
[20] K. Takeda, T. Kobayashi, J. Membr. Sci. 275 (2006) 61.
[21] L.N. Vandenberg, R. Hauser, M. Marcus, Reprod. Toxicol. 24 (2007) 139.
[22] V. Chauke, F. Matemadombo, T. Nyokong, J. Hazard Mater. 178 (2010) 180.
[23] H. -S. Yin, Y.-L. Zhou, S.-Y. Ai, J. Electroanal. Chem. 626 (2009) 626 80.
[24] H.-S. Yin, Y. Zhou, S.-Y. Ai, L. Cui, L. Zhu, Anal. Chim. Acta 659 (2010) 144.
[25] V. Chauke, T. Nyokong, Inorg. Chim. Acta 363 (2010) 3662.
[26] J. Liu, A.G. Rinzla, H. Dai, J.H. Hafner, R.K. Bradley, P.J. Boul, A. Lu, T. Iverson, K. Shelimov, C.B. Huffman, F. Rodriguez-Macias, T. Y-Seon Shon, R. Lee, D.T. Cobert, R.E. Smalley, Science 280 (1998) 1253.
[27] M. Brust, M. Walker, D. Bethell, D.J. Schiffrin, R. Whyman, J. Chem. Soc. Commun. (1994) 801–802.
[28] V.P. Chauke, E. Antunes, W. Chidawanyika, T. Nyokong, J. Mol. Cat. A: Chem. 335 (2011) 121.
[29] P. Tau, T. Nyokong, J. Porphyrins Phthalocyanines 10 (2006) 69.
[30] M.J. Stillman, T. Nyokong, in: A.B.P. Lever, C.C. Leznoff (Eds.), Phthalocyanines Properties and Applications, vol. 1, VCH Publishers, New York, 1989, p. 133.
[31] T. Nyokong, in: J. Jiang (Ed.), Functional Phthalocyanine Molecular Materials, Springer, New York, 2010, p. 94.
[32] S. Sapra, D.D. Sarma, Pramana 65 (2005) 565.
[33] T. García, E. Casero, M. Revenga-Parra, J. Martín-Benito, F. Pariente, L. Vázquez, E. Lorenzo, Biosens. Bioelect. 24 (2008) 184.
[34] L. Wang, W. Mao, D. Ni, J. Di, Y. Wu, Y. Tu, Electrochem. Commun. 10 (2008) 673.
[35] G.K. Ahirwal, C.K. Mitra, Sensors 9 (2009) 881.
[36] A.J. Bard, L.R. Faulkner (Eds.), Electrochemical Methods: Fundamentals and Application, Wiley, New York, 1980.
[37] J.J. Gooding, V.G. Praig, E.A.H. Hall, Anal. Chem. 70 (1998) 2396.
[38] Z. Li, M. Lieberman, Supramol. Sci. 5 (1998) 485.
[39] S. Trevin, F. Bedioui, M.G. Gomez Villegas, C. Bied-Charreton, J. Mater. Chem. 7 (1997) 923.